

# Numerical Investigation of Gas Channel Geometry of Proton Exchange Membrane Fuel Cell

H. Sadeghi<sup>1\*</sup>, I. Mirzaee<sup>1</sup>, S. Khalilarya<sup>1</sup> and N. Ahmadi<sup>2</sup>

1. Faculty of mechanical engineering, Urmia university, Urmia, Iran.  
2. Faculty of mechanical engineering, Urmia university of technology, Urmia, Iran.

Receive Date 12 December 2019; Revised 4 January 2020; Accepted Date 15 January 2020  
\*Corresponding author: h.sadeghi@msn.com (H. Sadeghi)

## Abstract

In the present research work, a 3D single-phase proton-exchange membrane fuel cell is simulated numerically. The governing equations are solved using the finite volume scheme, and the results obtained are validated against famous published data that show a proper conformity. The basic target is to investigate the gas channel shape effect on the cell performance and the mass transport phenomenon. First, the beside walls of the gas channels are converted from the straight condition to the sinusoidal form with two different steps, and in continuation, the membrane electrode assembly is bended in four states but the gas channel cross-section area is kept 1 mm<sup>2</sup>. The results obtained reveal that the spiral models because of a curved construction prepare a long pathway for the incoming gases, and also much mass diffusion to the reaction area. Thus for model M1, the produced current density for  $V = 0.6$  [V] increase by about 7.5%, and consequently, more oxygen and hydrogen is consumed. The pressure drop of the spiral models is studied; the results show that the base model has a less pressure drop but model M2 because of a higher performance and nearly the same pressure drop can be the best choice for the user. Also for the new bended models, the best choice is the model with  $\delta = 0.4$ , which has produced more current density, while its reaction area is about 19.64 mm<sup>2</sup> larger than the conventional model with  $\delta = 0$ .

**Keywords:** Geometrical configuration; PEM fuel cell; Gas channel; Species distribution; Membrane electrode assembly.

## 1. Introduction

Hydrogen fuel can burn with oxygen without any pollutant emission. Thus it can be the best candidate for green power sources. On the other hand, hydrogen is the main fuel of the fuel cells, in which, because of the electrochemical reactions between hydrogen and oxygen, the electrical energy can be extracted.

The other products of the mentioned reaction are heat and water. Heat can be used in power plants and water can be used in the liquid or vapor form. Generally, cleanliness is one of the most important characteristics of fuel cells. Among the different types of fuel cells, the Proton Exchange Membrane Fuel Cell (PEMFC) is a low-temperature one that leads to low heat stresses [1]. On the other hand, due to a high power density, it is a favorable option for the future power generation technologies.

The geometrical configuration of fuel cells affects the performance. Therefore, in the present work, the main focus was on the gas channel geometry.

Among the investigated problems, the conversion of channels to the curved and also bended conditions were done.

The researchers have concentrated on different aspects of the fuel cell performance enhancement. Rezazadeh and Ahmadi [2, 3] have studied the numerical models, and some vital information about the mass transport phenomena and reaction rate in a fuel cell has been reported. The effect of semi-circular prominences on the gas diffusion layers has been studied with more details. Ahmadi *et al.* [4] have presented a model with circular and elliptical cross-sections and have solved the continuity and momentum equations analytically with the perturbation method. The main goal of the mentioned work was to investigate the geometrical configuration effect on the PEMFC performance. Zhuqian Zhang *et al.* [5] have published a mathematical model. In this 3D model, temperature distribution liquid water transport processes have

been discussed. The results obtained have revealed that a relatively high operating temperature increases electrode kinetics and reduces liquid water saturation, which also improves fuel cell performance. Dutta *et al.* have suggested the first 3D for PEMFC [6]. Their predictions show that the inclusion of a gas diffusion layer produces a lower and uniform current density than the cases without diffusion layers. In continuation, the results illustrate that the membrane thickness and cell voltage have significant effects on the axial distribution of the current density and net rate of water transport. Wang *et al.* have studied a serpentine flow slab in proton exchange membrane fuel cells [7]. The results obtained revealed that the performance in the model with convergent-type serpentine flow slab was better than that of serpentine flow slab with a constant duct channel. Yang *et al.* [8] have improved the performance of PEMFC. In this work, various electrodes fabricated using different fabrication procedures and the CO presence effect were investigated at the anode interface. Ahamr *et al.* [9] have studied the circular tubular PEMFC using different architectures and numbers of layers, and investigated the performance improvement. Carral *et al.* [10] have applied a finite element technique to simulate PEMFC stack and studied the number of cells and their position numerically. The results obtained revealed that a proper uniformity of the MEA compression was achieved with the greatest number of cells, and at the stack center. Ahmadi *et al.* [11] have numerically and experimentally studied a PEM fuel cell. Their results indicated that if the gas diffusion layer prominence radius was 0.45 mm, the optimum performance was extracted. They also investigated the number of channels, and concluded that 3 channels produced a higher current density. The results obtained showed a noticeable increase in the current density at the similar cell voltages, in comparison with the base model. Rezazadeh *et al.* [12] have developed a 3D and single-phase CFD model of a PEMFC. The important goal of this research work was to investigate the serpentine channel performance compared with the conventional straight channels. In the present work, a 3D numerical investigation of a novel curved gas channel shape effect on the efficiency and mass transport of a PEM fuel cell was done. In the proposed models, the beside walls of the gas channels were converted from a straight

form to the sinusoidal shape with different steps. The aim was to compare the proposed models with the base conventional model from the viewpoint of species and other vital parameter distributions. Some important parameters such as the species mass fractions, cell temperature, and current density were presented for the models in more details. The numerical results revealed that the new proposed models operated better and produced a higher current density than the base model. On the other hand, the pressure drop was studied. Because of the long pathway of the incoming gases in the new models, the mentioned parameter was higher. Finally, the model M1 with about 7.5% higher current density at  $V = 0.6$  [V] was compared with the conventional model; it was the best choice. On the other hand, between the four bended models, the case with  $\delta = 0.4$  had the optimum condition and produced a higher performance.

## 2. Mathematical model

Figure 1 shows a schematic representation of the mono cell of a PEMFC (base model). It includes two porous gas diffusion layers, a polymer electrolyte membrane, two catalyst layers, two gas channels, and bipolar plates. The membrane part is surrounded by the anode and cathode gas channels. Figure 2 illustrates the cell without bipolar plates. The following simplifications were applied to govern the equation:

- All gases are considered as ideal.
- The GDLs and catalyst layers are homogeneous porous media.
- The fluid flow is incompressible and laminar ( $Re \leq 200$ ).
- The volume of liquid-phase water in the domain is not notable, so the flow field is in a single phase (just the vapor phase of water is considered).

## 3. Governing equations

In the present work, the model formulation was done for a single domain and the governing equations were solved by the computational fluid dynamics technique. The mentioned governing equations consist of mass conservation, momentum, species, charge, and energy equations that are discretized with the finite volume method and can be written as follow [11]:

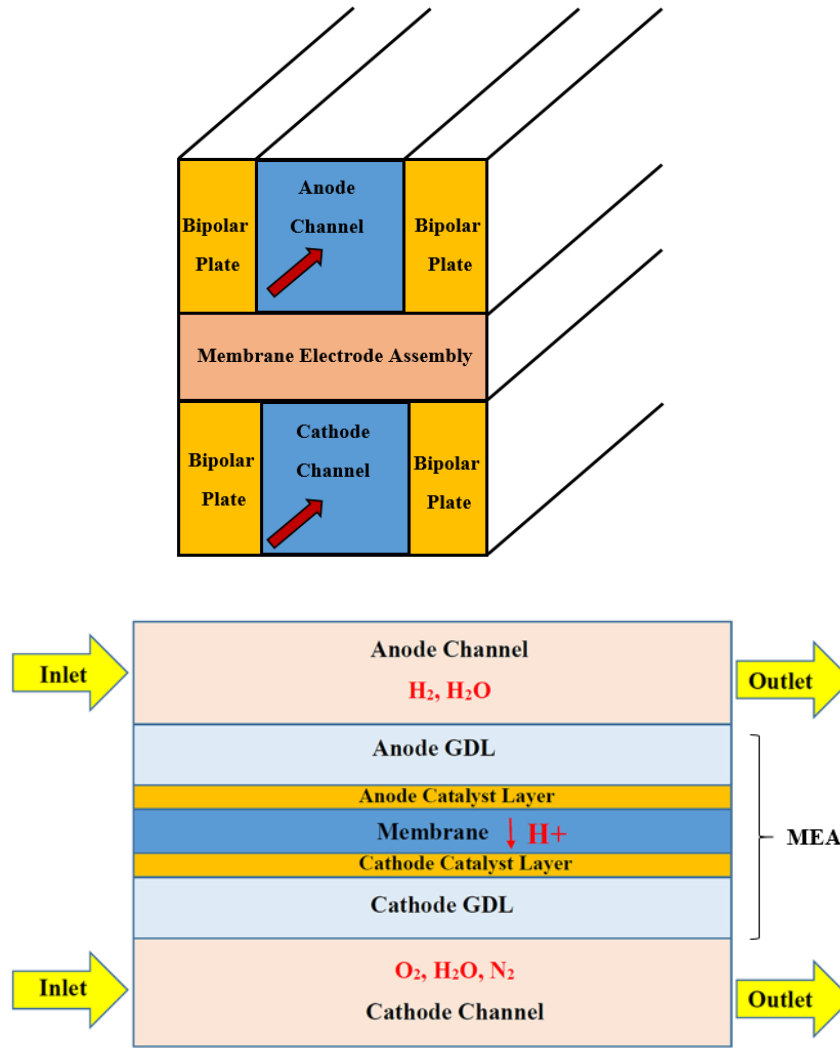


Figure 1. Schematic representation of proton exchange membrane fuel cell (the upper one is a 3D view and the other one is a side cross-section).

$$(\nabla \cdot \rho \mathbf{u}) = 0 \quad (1)$$

$$\frac{1}{(\varepsilon^{eff})^2} \nabla \cdot (\rho \mathbf{u} \mathbf{u}) = -\nabla P + \nabla \cdot (\mu \nabla \mathbf{u}) + S_u \quad (2)$$

$$\nabla \cdot (\mathbf{u} C_K) = \nabla \cdot (D_K^{eff} \nabla C_K) + S_K \quad (3)$$

$$\nabla \cdot (K_e^{eff} \nabla \Phi_e) + S_\Phi = 0 \quad (4)$$

$$\nabla \cdot (\rho u T) = \nabla \cdot (\lambda_{eff} \nabla T) + S_T \quad (5)$$

In Equation (1), the mixture density has been illustrated with  $\rho$ .  $\varepsilon^{eff}$  is the effective porosity inside the porous sections, and the viscosity of the mixture is shown as  $\mu$  in Eq. (2).  $S_u$  is the source term, and is used to describe Darcy's drag inside porous layers.  $C_K$  is the species concentration, and

also  $D_K^{eff}$  is the species effective diffusion coefficient.

More information about the governing equations and source terms is available in references 11-18.

#### 4. Boundary conditions

The mentioned governing equations are solved using the finite volume method and also the proper boundary conditions [11]. The boundary conditions are specified at the extrinsic boundaries including:

1. Mass flow rate at the entry of channels is constant.
2. Pressure at the channels' outlet is constant and equal to the atmospheric pressure.
3. For the mass, momentum, species, and potential equations, no-flux conditions are implemented at all external surfaces, except for gas inlets and outlets in the flow channels for both the anode and cathode sides.

### 5. Numerical implementation

In order to solve the governing equations numerically with the related boundary conditions, the implicit finite volume method was used to discretize the partial derivatives. The SIMPLE algorithm was adopted for the pressure correction equation. The iterative methods were used to solve the resultant algebraic equations. The calculations were repeated in each time step until the convergence criterion was met. The convergence criterion reads as the relative error to be less than  $10^{-9}$ .

The number of iterations is about 5000 for a higher cell voltage difference and 14,000 for a lower one. Thus the maximum time for converging the solution for a low cell voltage is about 18 hours. Figure 2 illustrates the numerical procedure implementation algorithm with more details.

Table 1 indicates the boundary condition for different parts of the cell completely.

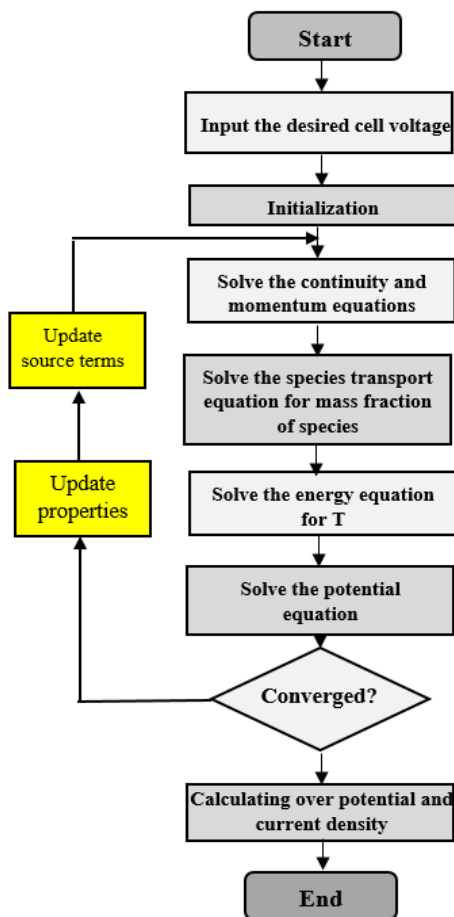


Figure 2. Numerical procedure algorithm.

### 6. Model Validation

In order to validate the introduced model, the numerical results obtained for the base conventional case (with straight gas channels) were

compared with the experimental data represented by Ticianelli *et al.* [13]. Figure 3a shows a favorable agreement between them.

The fuel cell operating condition and geometric parameters are listed in table 2. The incoming gases are in a fully humidified condition.

In order to analyze the presented numerical model, the structured quad meshes were applied and in the catalyst layers' zones; where the electrochemical reactions occur, the meshes are finer. On the other hand, the grid independency procedure was done, and finally, the usable mesh was chosen (figure 3b). According to the results obtained from 240000 to more other cells, the same output was extracted, and therefore, for a low computation time and a fast convergence, 240000 cells were chosen as the best and useful ones. The finite volume method was used for discretizing and solving the governing equations. Because of some assumptions such as water in single-phase, there was a numerical error, especially at low cell voltages. Figure 4 shows the oxygen and water mass fraction at the cathode catalyst and membrane interface at  $V = 0.4$  [V] for different mesh numbers, which indicates and confirms the mesh independency.

Figures 5a and 5b show the oxygen mass fraction in lateral distance between the membrane and the cathode catalyst layer in three different cross-sections and two cell voltages for the base model. It is clear that at a low cell voltage and consequently high current density, the oxygen consumption will be high. Thus in  $V = 0.4$  [V], the oxygen magnitude is lower. Meanwhile, at the shoulder regions (below bipolar plates), the oxygen consumption rate is faster because those regions are shorter paths for the electrons to reach.

Table 2. Geometrical parameters and operating conditions [13].

Parameter	Value
Anode & cathode pressure	3 atm.
Anode & cathode humidity	100%
Gas channel length	$7.0 \times 10^{-2}$ m
Gas channel width and depth	$1.0 \times 10^{-3}$ m
Bipolar plate width	$5.0 \times 10^{-4}$ m
Gas diffusion layer thickness	$3.0 \times 10^{-4}$ m
Catalyst layer thickness	$1.29 \times 10^{-5}$ m
Membrane thickness	$108 \times 10^{-6}$ m
Cell temperature	70 °C
Porosity	0.4
Stoichiometry	2

**Table 1. Boundary condition for different parts of the cell.**

Type of boundary condition	Type of zone in PEMFC geometry
$u = u_{in}, T = T_{in}, v = 0, C_{H_2} = C^a_{H_2,in}, C_{H_2O} = C^a_{H_2O,in}$	Anode gas channel inlet
$u = u_{in}, T = T_{in}, v = 0, C_{O_2} = C^c_{O_2,in}, C_{N_2} = C^c_{N_2,in}$	cathode gas channel inlet
$\frac{\partial u}{\partial x} = \frac{\partial v}{\partial x} = \frac{\partial w}{\partial z} = \frac{\partial T}{\partial x} = 0$	Anode and cathode gas channel outlet
$\frac{\partial u}{\partial y}_{y=h_1^-} = \varepsilon_{eff,GDL} \frac{\partial u}{\partial y}_{y=h_1^+}, \frac{\partial v}{\partial y}_{y=h_1^-} = \varepsilon_{eff,GDL} \frac{\partial v}{\partial y}_{y=h_1^+}$ $\frac{\partial w}{\partial y}_{y=h_1^-} = \varepsilon_{eff,GDL} \frac{\partial w}{\partial y}_{y=h_1^+}$	GDL and gas channels interface
$\varepsilon_{eff,GDL} \frac{\partial u}{\partial y}_{y=h_2^-} = \varepsilon_{eff,CL} \frac{\partial u}{\partial y}_{y=h_2^+}, \varepsilon_{eff,GDL} \frac{\partial v}{\partial y}_{y=h_2^-} = \varepsilon_{eff,CL} \frac{\partial v}{\partial y}_{y=h_2^+},$ $\varepsilon_{eff,GDL} \frac{\partial w}{\partial y}_{y=h_2^-} = \varepsilon_{eff,CL} \frac{\partial w}{\partial y}_{y=h_2^+}$	GDL and CTL interface
$u = v = w = C_i = 0$	Membrane and CTL interface
$u = v = w = C_i = 0, T_{surface} = 353K$	Top surface of gas channel
$u = w = 0, T_{surface} = T_{wall}$	Bottom surface of gas channel
$\phi_{sol} = 0, \frac{\partial \phi_{mem}}{\partial y} = 0$	Top surface of anode bipolar
$\phi_{sol} = V_{cell}, \frac{\partial \phi_{mem}}{\partial y} = 0$	Top surface of cathode bipolar
$\frac{\partial \phi_{mem}}{\partial x} = 0, \frac{\partial \phi_{mem}}{\partial z} = 0, \frac{\partial \phi_{sol}}{\partial x} = 0, \frac{\partial \phi_{sol}}{\partial z} = 0$	External surfaces

The letter “h” above equation denotes the layer thickness and “z” is the flow direction.

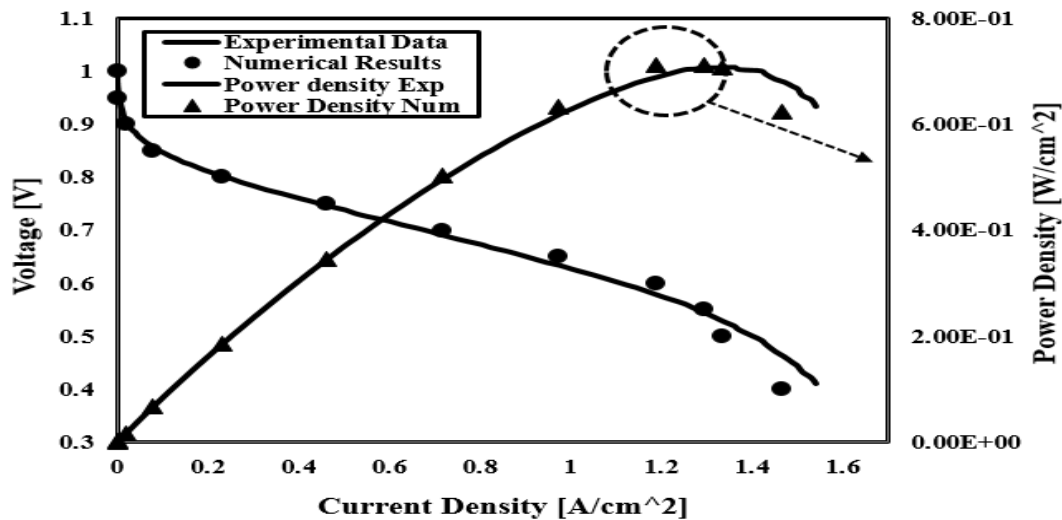


**Figure 3a. Polarization curve of model validation.**

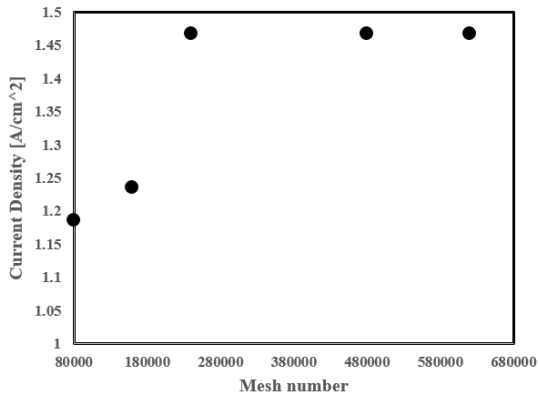


Figure 3b. Mesh independency test for  $V = 0.4$  [V].

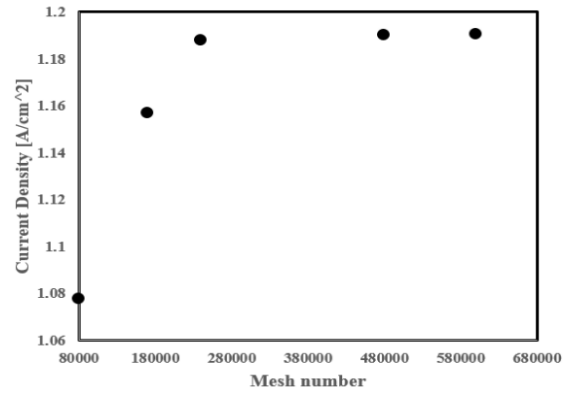


Figure 3b. Mesh independency test for  $V = 0.6$  [V].

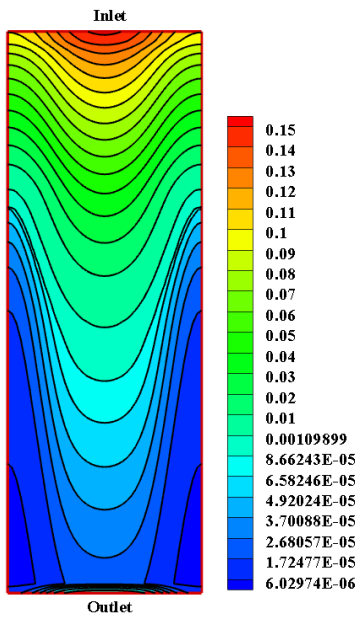


Figure 4a. Oxygen mass fraction for 240000 meshes.

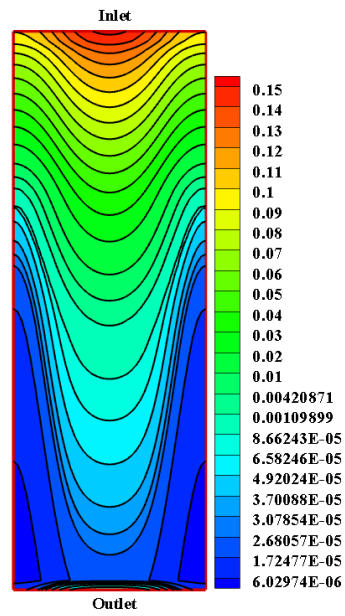


Figure 4a. Oxygen mass fraction for 480000 meshes.

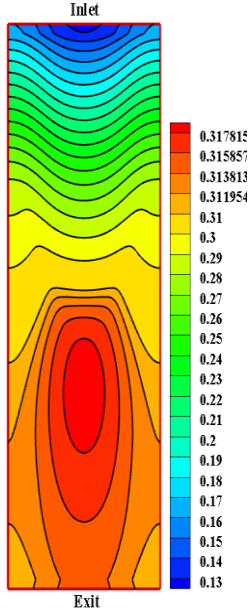


Figure 4b. Water mass fraction for 240000 meshes.

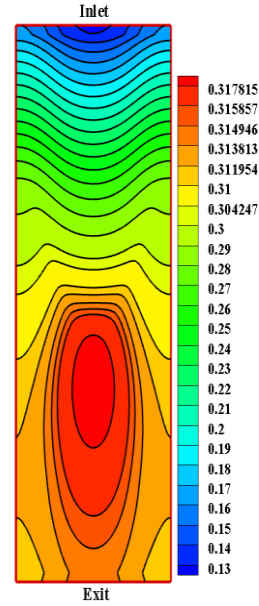


Figure 4b. Water mass fraction for 480000 meshes.

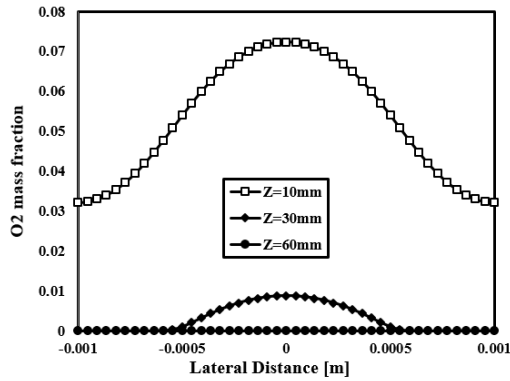


Figure 5a. O<sub>2</sub> mass fraction at V = 0.4 [V].

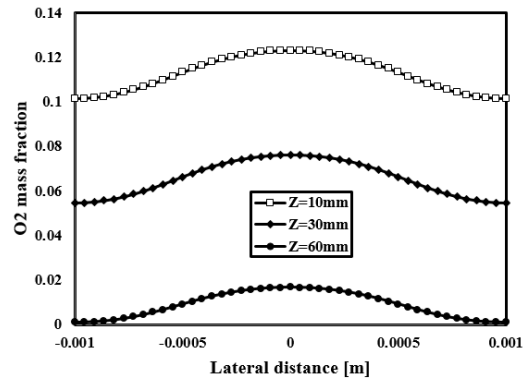


Figure 5b. O<sub>2</sub> mass fraction at V = 0.6 [V].

A more oxygen consumption means a high water production. Therefore, according to figures 6a and 6b, it can be said that there is a reverse relation between oxygen and water mass fractions. Water magnitude in the shoulder regions is high because

of high oxygen consumption there. Also for a low cell voltage, more water is produced because of a faster electrochemical reaction rate. The contour of water mass fraction at V = 0.4 [V] can be found in figure 4b.

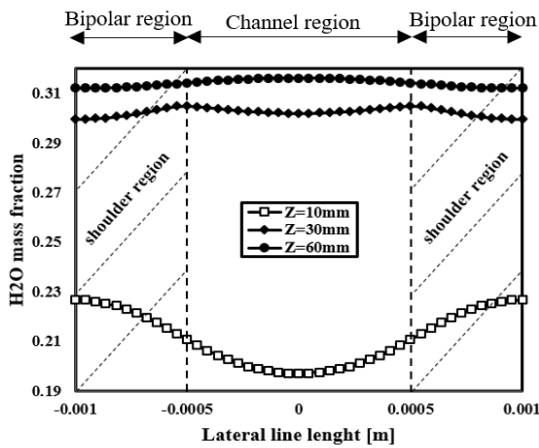


Figure 6a. H<sub>2</sub>O mass fraction at V = 0.4 [V].

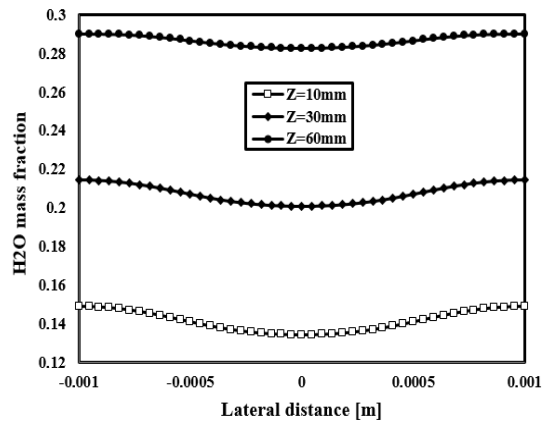


Figure 6b. H<sub>2</sub>O mass fraction at V = 0.6 [V].

Figures 7a and 7b illustrate the oxygen and water mass fraction along the cell between the membrane and the cathode catalyst layer for different cell voltages. As it is clear, the oxygen along the the cell

has been consumed, and inversely, the water has been produced. While the cell voltage decreases, the oxygen magnitude decreases and the amount of water increases.

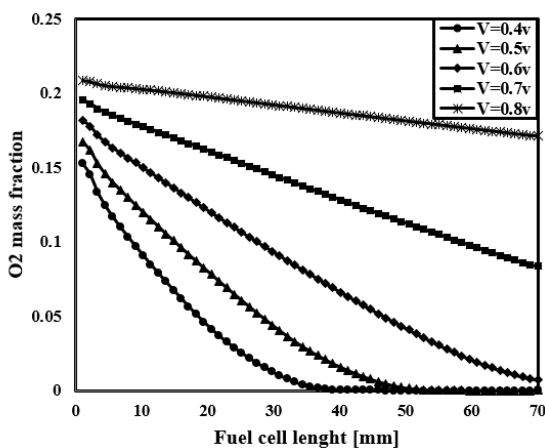


Figure 7a. O<sub>2</sub> mass fraction along the cell.

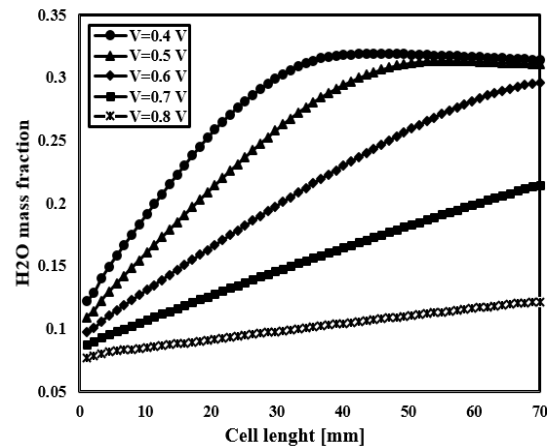


Figure 7b. H<sub>2</sub>O mass fraction along the cell.

Figure 8 indicates the water mass fraction along the cell between the membrane and the anode catalyst layer. The diagram shows that water decreases along the cell and also by decreasing the cell voltage. While the cell voltage becomes lower, the current density becomes higher and more water molecules try to transfer  $H^+$  toward the cathode side to complete the electrochemical reaction. Thus by increasing the current density, more anode side water molecules immigrate toward the cathode side, and consequently, there is a lack of water at the anode side. Figures 9a and 9b illustrate the temperature distribution, which confirms the above explanations. A low cell voltage results in a high reaction rate and more heat generation. Also from inlet to exit, the temperature decreases because of water presence and good thermal conductivity of bipolar plates. Therefore, at the shoulder region, the temperature is lower.

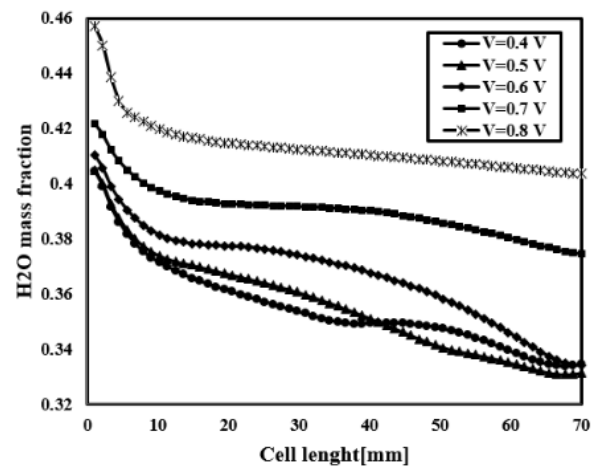


Figure 8. H<sub>2</sub>O mass fraction along the cell at the anode side.

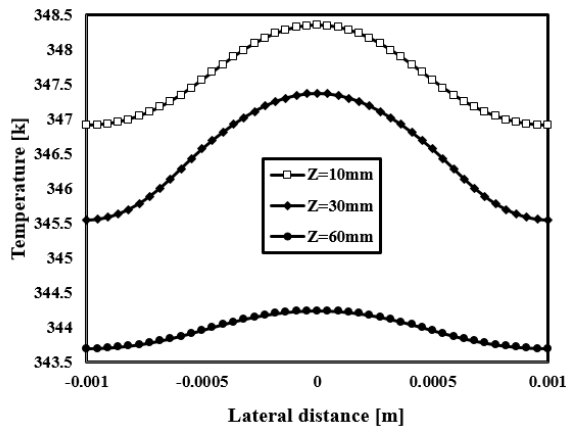


Figure 9a. Temperature distribution at V = 0.4 [V].

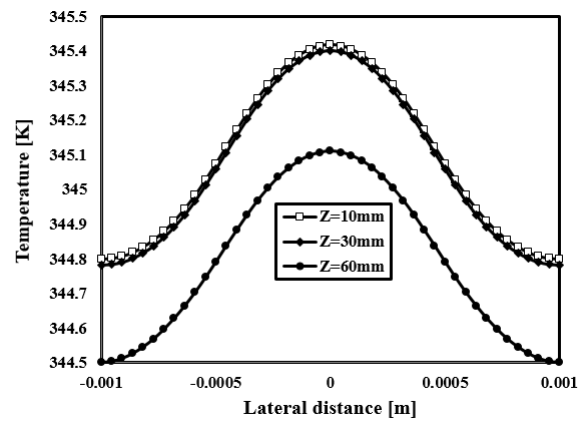


Figure 9b. Temperature distribution at V = 0.6 [V].

The current density distribution decreases from inlet to exit because the reaction rate along the cell diminishes (figures 10a and 10b). Also it is clear

that at the bipolar regions, the current density is high because the electrons enter the shoulder region from the mentioned location.

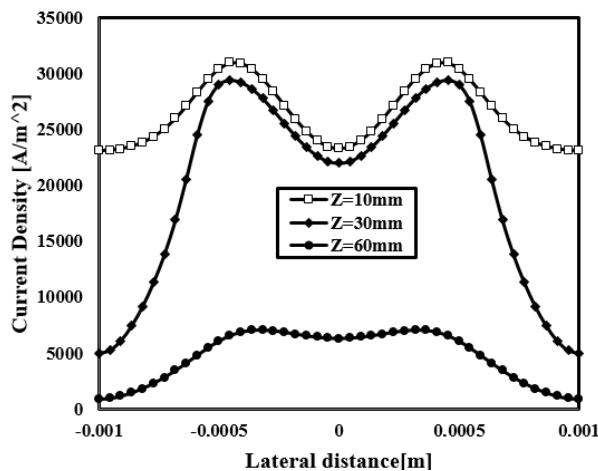


Figure 10a. Current density distribution at V = 0.4 [V].

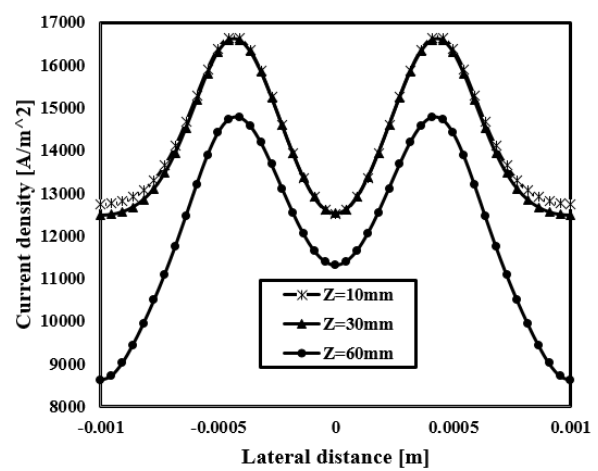


Figure 10b. Current density distribution at V = 0.6 [V].

Another important parameter that directly relates to the oxygen mass fraction is the cathode overpotential (COP). COP is a kind of voltage loss that

is influenced by the presence or lack of oxygen. While there is a lack of oxygen, COP will be higher; this is shown in figures 11a and 11b. On the

other hand, the ohmic loss distribution that is related to the protonic conductivity and membrane

thickness [11] is illustrated in figures 11c and 11d.

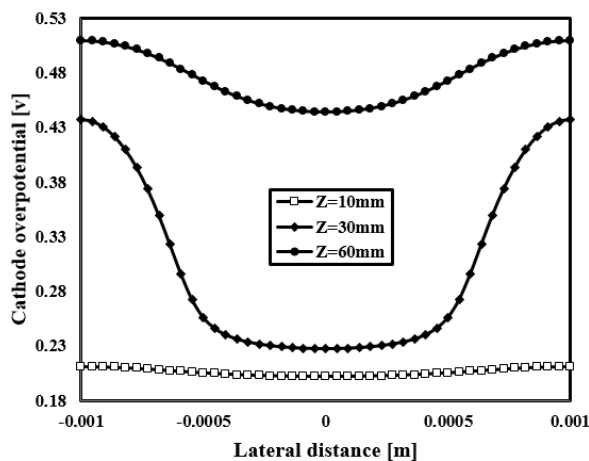


Figure 11a. COP distribution at V = 0.4 [V].

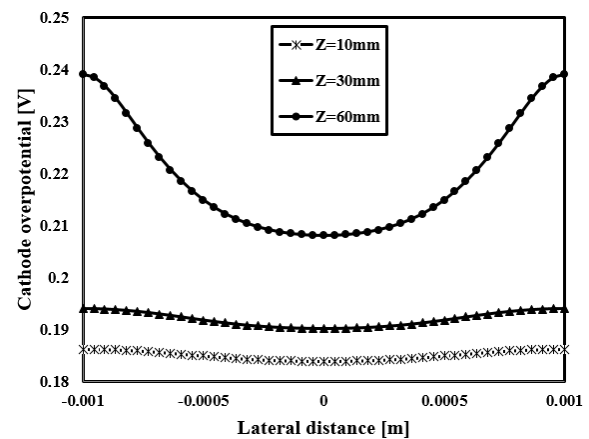


Figure 11b. COP distribution at V = 0.6 [V].

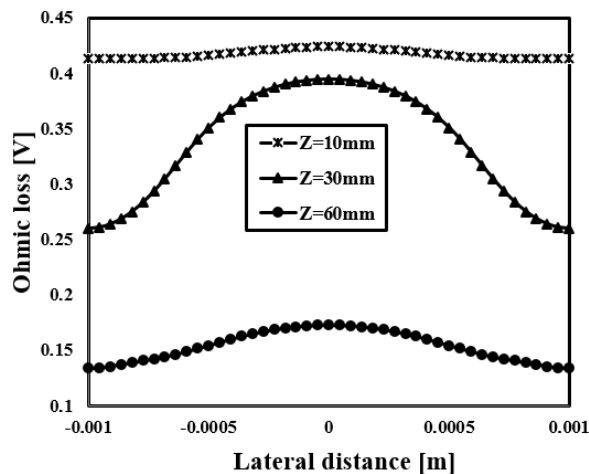


Figure 11c. Ohmic loss distribution at V = 0.4 [V].

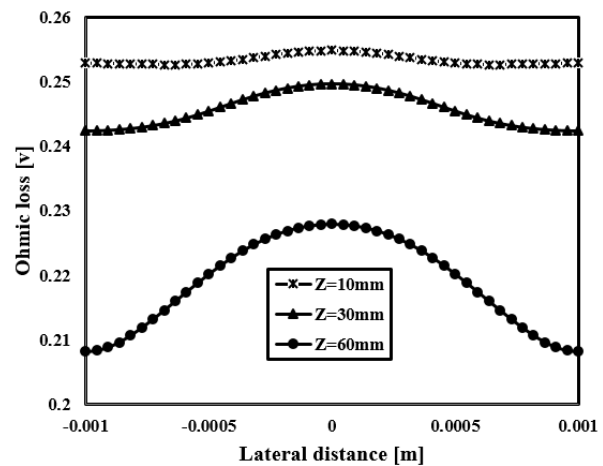


Figure 11d. Ohmic loss distribution at V = 0.6 [V].

## 7. Proposed models

In the present work, as the new novel models, two kinds of wavy flow channels were simulated numerically. The mentioned new models, for the first time, were applied on the PEM fuel cell to investigate the performance enhancement and mass transport phenomenon. Figure 12 shows a view of these geometries. The mentioned models include 5 same arcs through the gas channel beside walls. In model 1 (M1), the arcs have the same steps and the gas channel geometry is symmetric. In model 2 (M2), the gas channel shape is sinusoidal. It is clear that in both new models, the radii of the arcs are the same and equal to 0.2 mm. Also the length of each arc in the Z direction is equal to 14 mm. In this way, the incoming fluid pathway inside the channels will be longer than the model with straight gas channels. The main goal of this work is to distinguish how the fluid pathway influences the species distribution and also the cell performance. Therefore, some important parameters such as O<sub>2</sub> and H<sub>2</sub>O mass fractions, temperature, and current

density distribution were calculated for the proposed models and compared with the base model results. The dashed lines illustrate the straight channel walls.

Figure 13 declares the current density magnitude of three models for two cell voltages (V = 0.6, 0.4 [V]). As it is clear, M1 has a better performance than the others because of its construction and kind of mass distribution on the GDL layers. On the other hand, the sinusoidal model (M2) has a higher performance than the base model because in the mentioned model, the species path from inlet to exit is longer, so they have enough time to diffuse toward the electrochemical reaction area. Briefly, the new models can produce more current density than the base model upon their geometrical conditions.

The oxygen mass fraction is an important parameter that can show the fuel cell ability to produce current density. Thus figure 14 demonstrates that M1 consumes more oxygen than the other models. It should be said that the

mentioned parameter was extracted along the line at the middle of the cell between the membrane and the cathode catalyst layer. Figures 15a, 15b, and 15c illustrate the oxygen distribution at different cross-sections of the cell. It should be said that for the base conventional model, just the MEA and

cathode side are shown but for the new models, the cross-sections consist of the whole MEA, and the anode and cathode sides. Consequently, more oxygen consumption leads to more water production; this can be seen in figure 15.

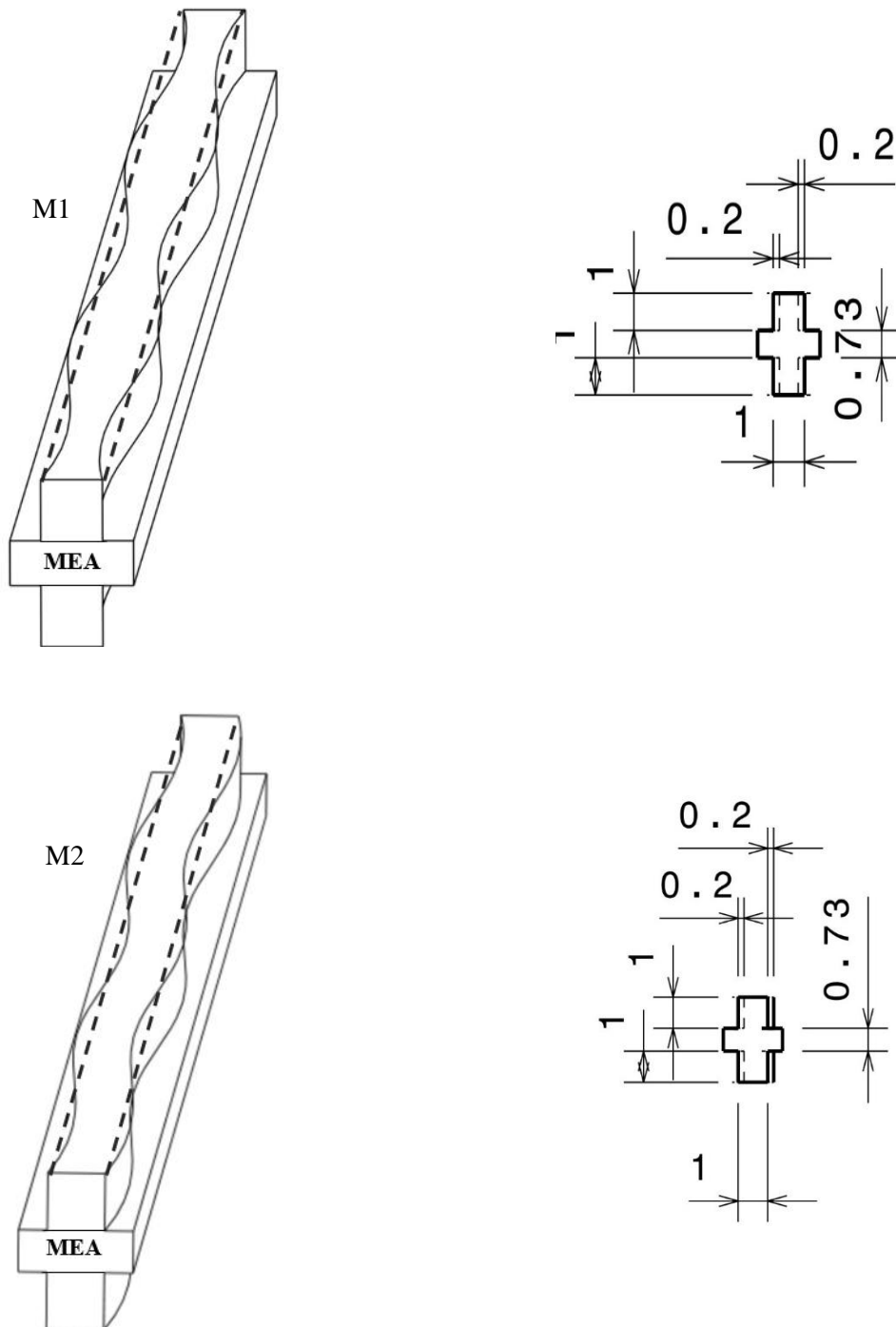


Figure 12. Schematic representations of the proposed models (the right ones are cross-section views without bipolar plates).

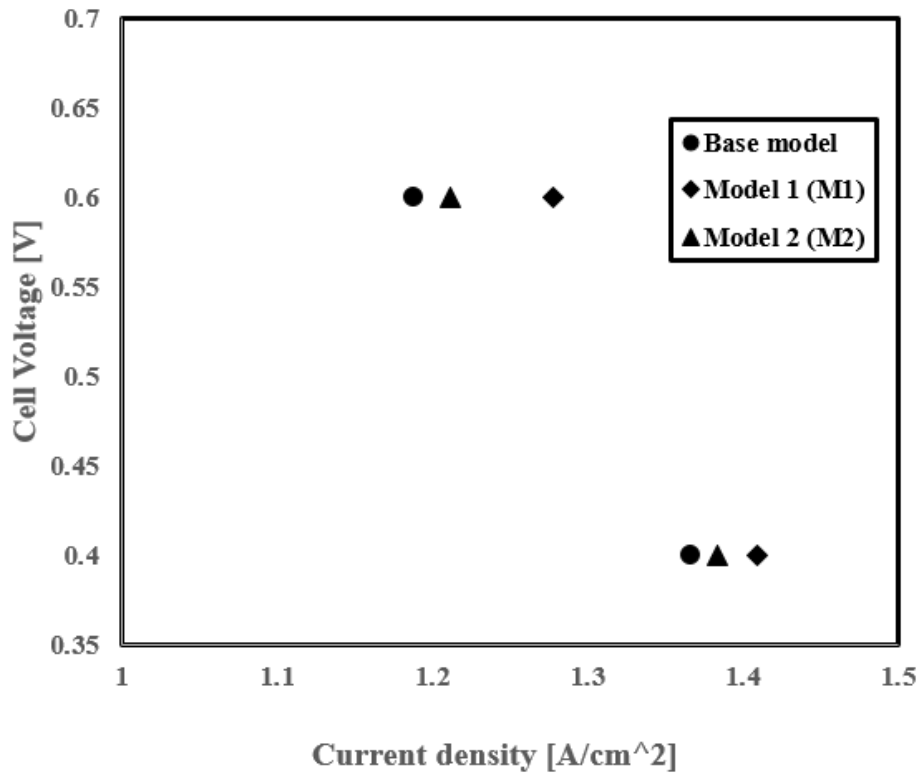


Figure 13. Comparison of model performances at V = 0.4 [V] and V = 0.6 [V].

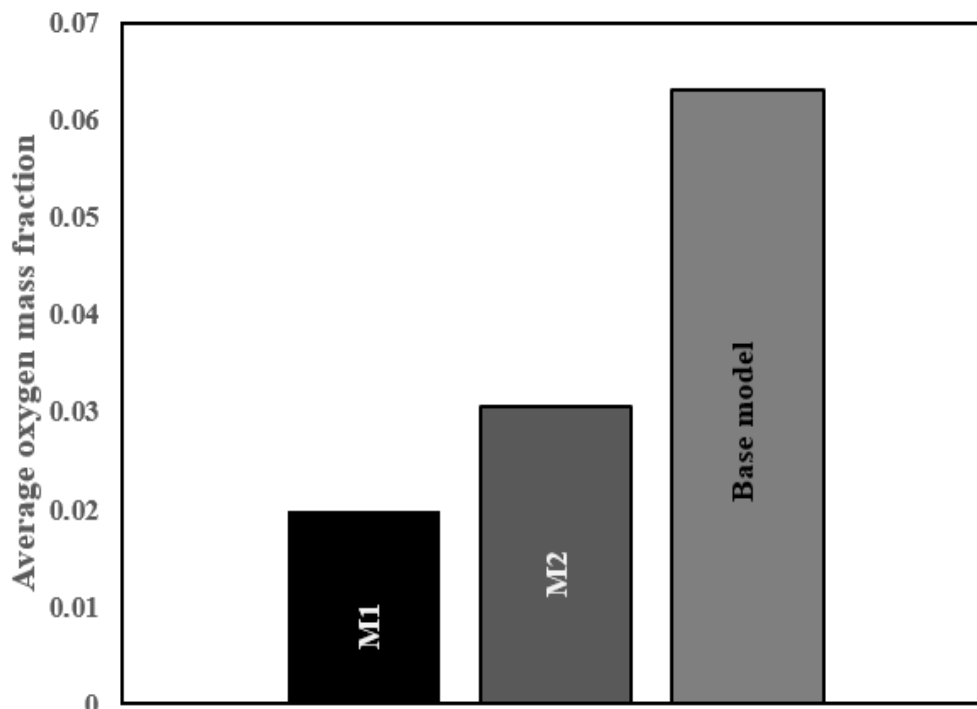


Figure 14. Average O<sub>2</sub> mass fraction along the cell for models at V = 0.6 [V].

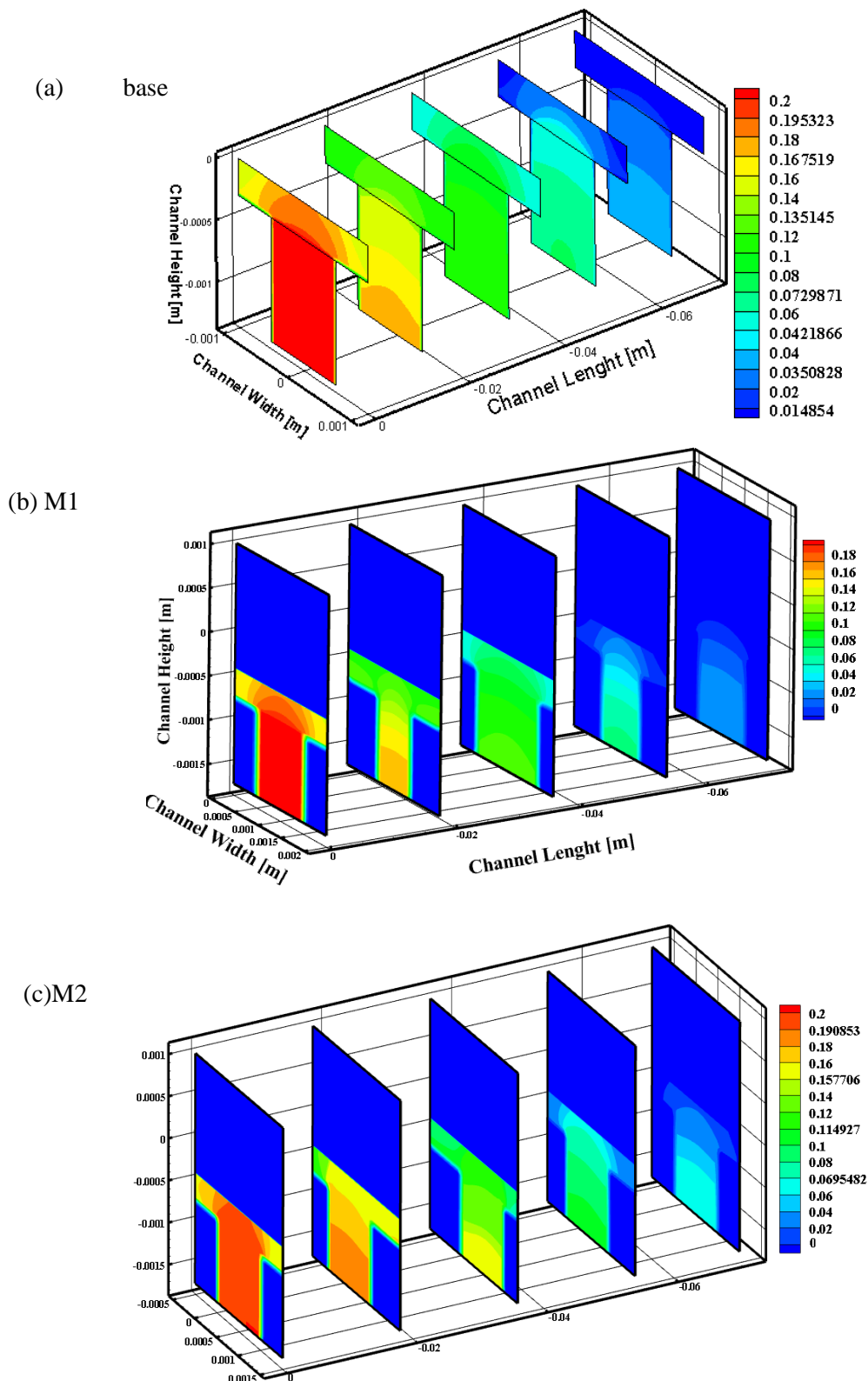


Figure 15. O<sub>2</sub> mass fraction at different cross-sections for the models at V = 0.6 [V].

Figure 16 shows the average water mass fraction along the line between the membrane and the cathode catalyst layer. M1 produces more water than the others. Contours of water distribution confirm this mentioned fact clearly (figure17). Figures 17b-1 and 17b-2 illustrate the water

distribution at cross-sections and the whole fuel cell, respectively. The trend shape of the M1 model is because of the gas channel geometry and also the line location on which the water mass fraction has been extracted.

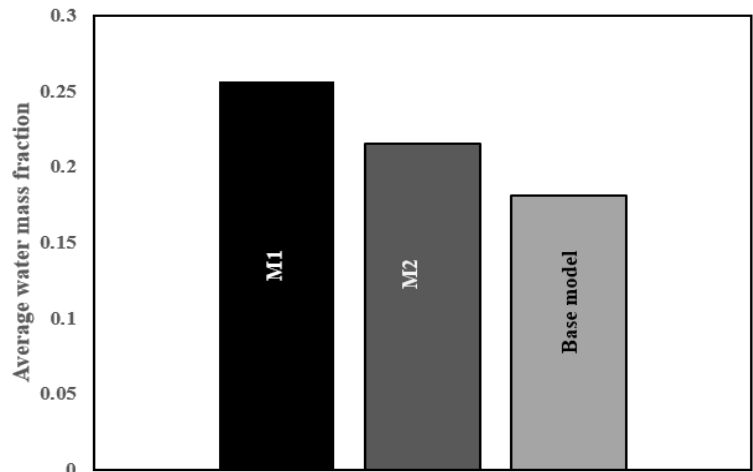
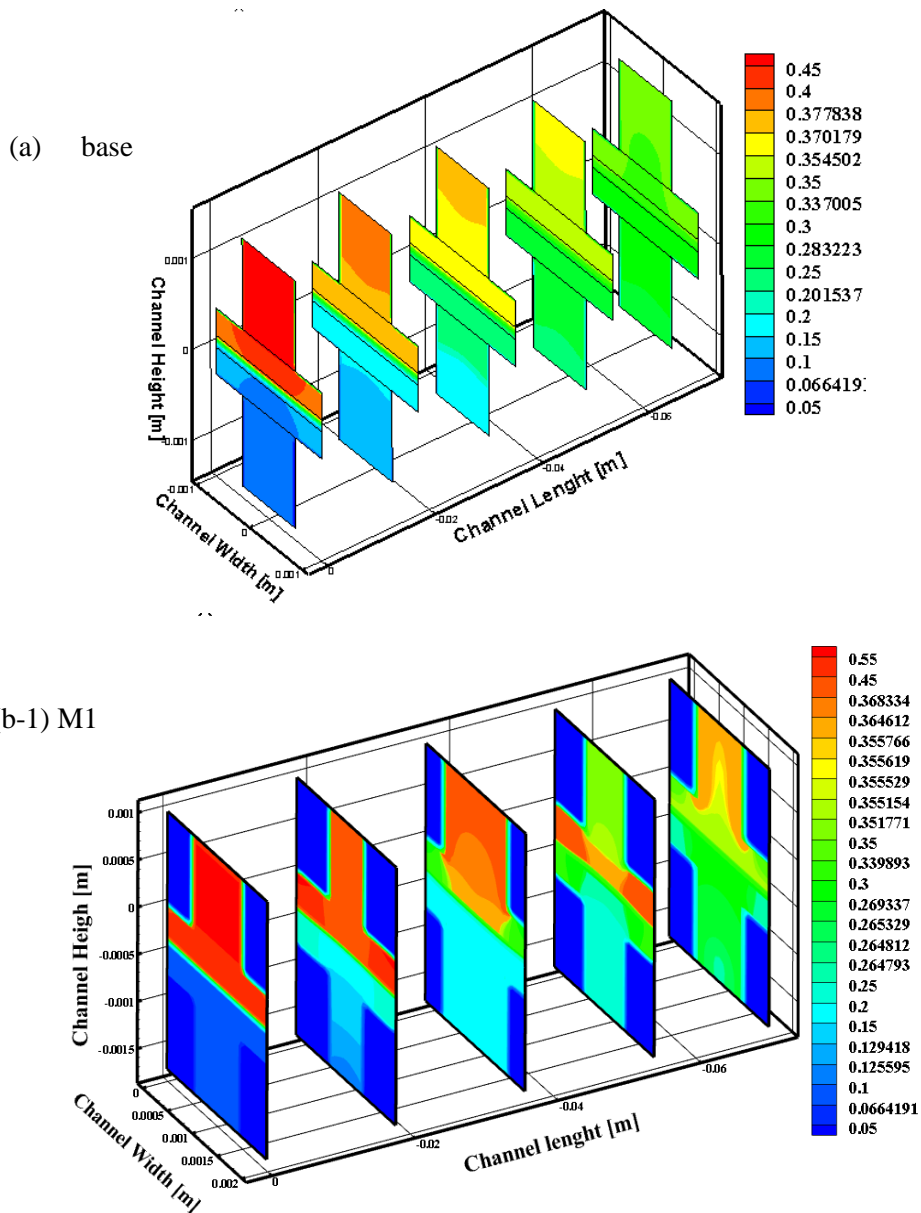
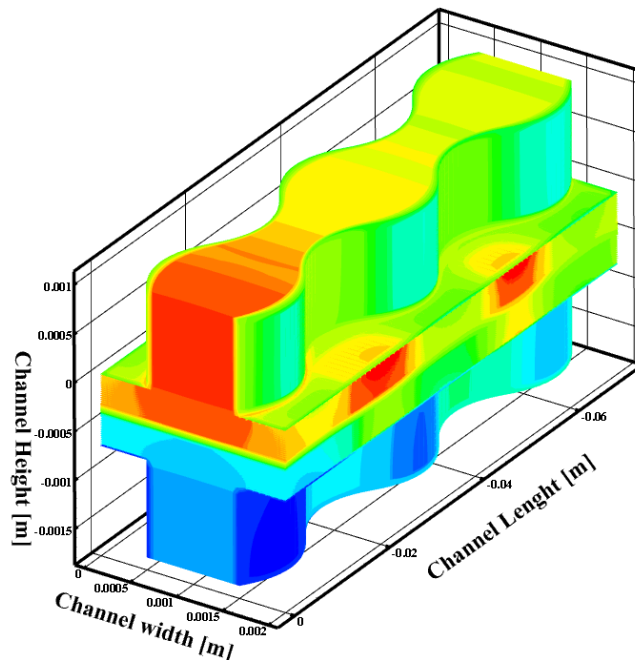


Figure 16. Average H<sub>2</sub>O mass fraction along the cell for models at V = 0.6 [V].



(b-2) M1



(c) M2

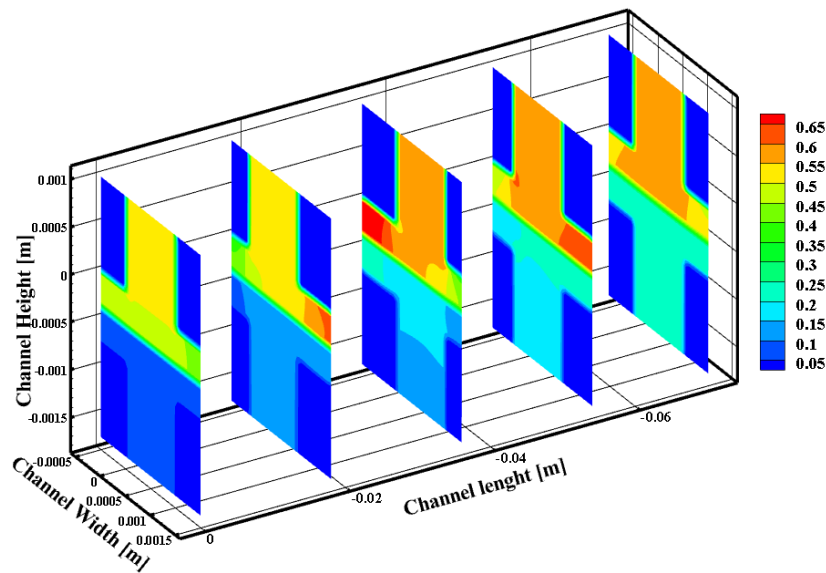


Figure 17. H<sub>2</sub>O mass fraction at different cross-sections for models at V = 0.6 [V].

The current density distribution along the cell between the membrane and the cathode catalyst layer (figure 18) defines that the M1 model is the best choice for the design and use in different

applications. Contours of current density distribution confirm the mentioned fact clearly (figure 19).

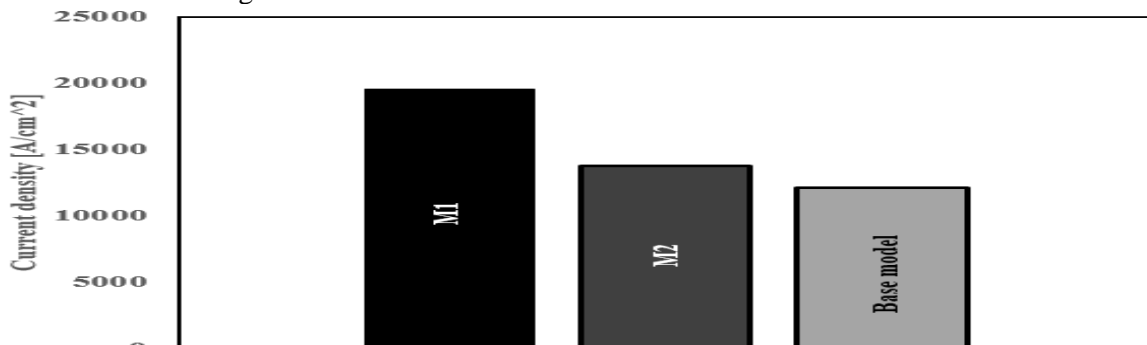


Figure 18. Average current density along the cell for models at V = 0.6 [V].

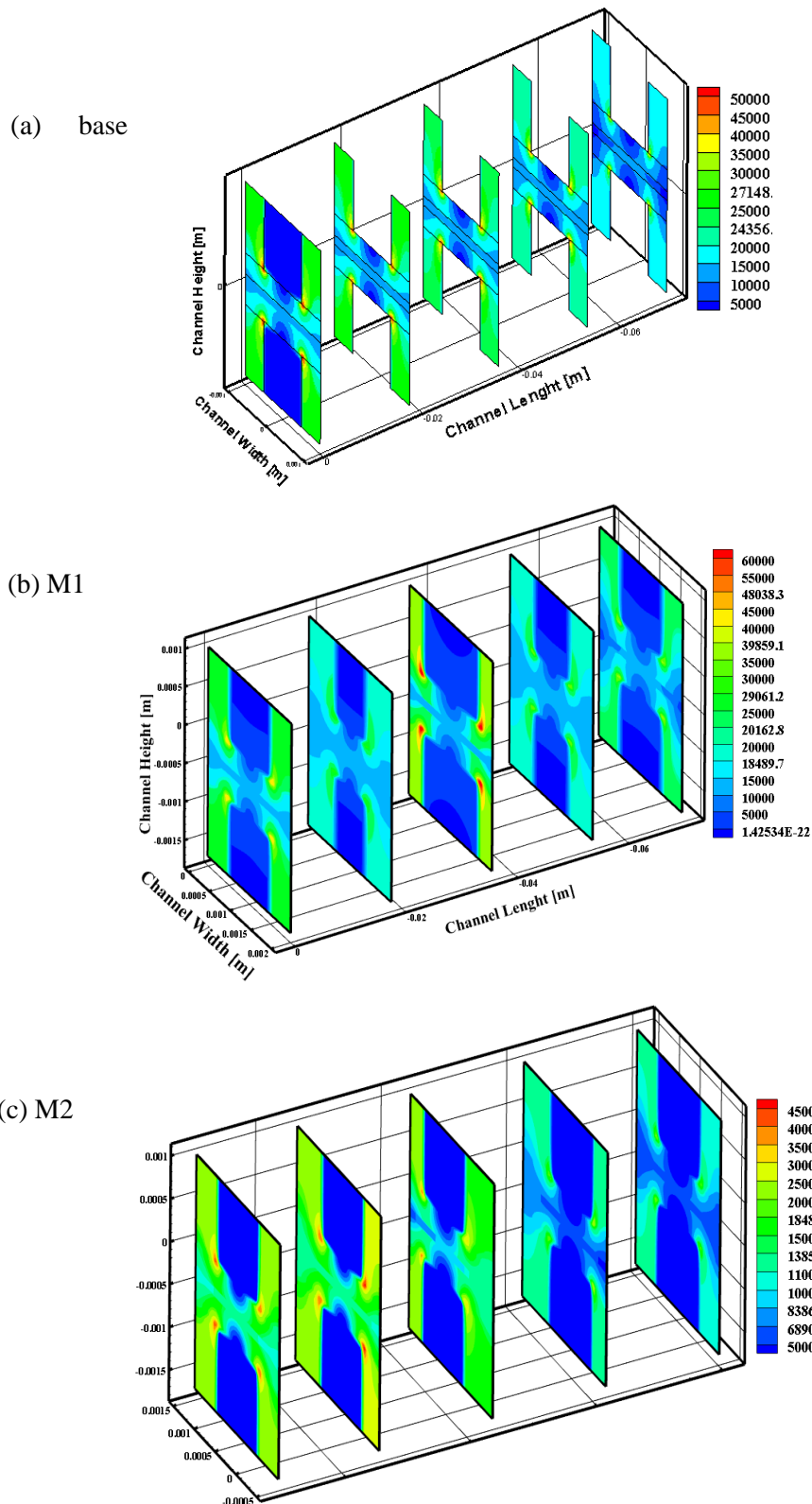


Figure 19. Current density distribution at different cross-sections for models at  $V = 0.6$  [V].

The average hydrogen mass fraction between the membrane and the anode catalyst layer is presented in figure 20. The result demonstrates that M1 consumes more hydrogen than the other models. Figure 21a, 21b, and 21c illustrate the hydrogen distribution at different cross-sections of the cell. It should be said that for the base conventional

model, just the MEA and cathode side have been shown but for the new models, the cross-sections consist of the whole MEA, and the anode and cathode sides. Less hydrogen means that the cell consumes much hydrogen, and more  $H^+$  is produced for participation in the electrochemical reaction.

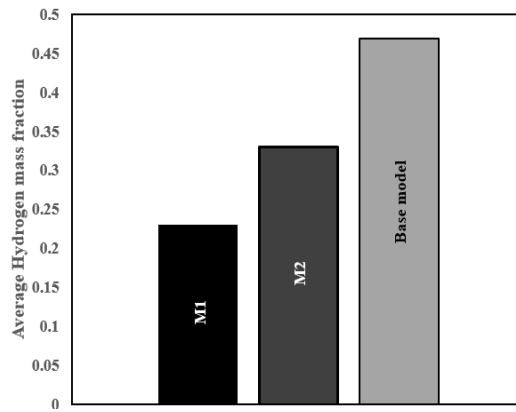
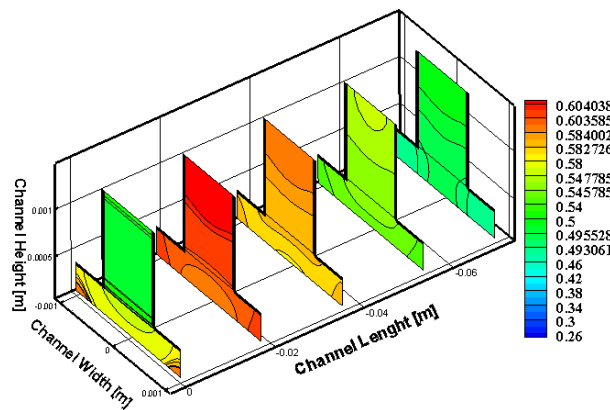
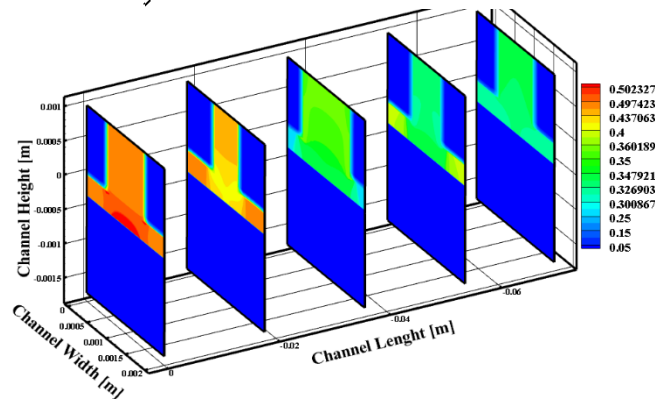


Figure 20. Average hydrogen mass fraction at V = 0.6 [V].

(a) base



(b) M1



(c) M2

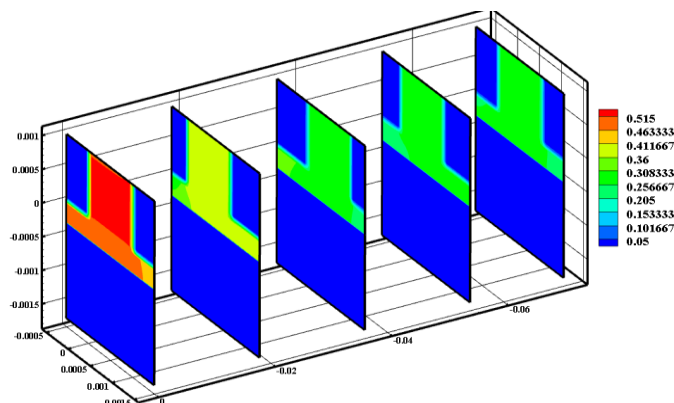


Figure 21. Hydrogen distribution at different cross-sections for models at V = 0.6 [V].

As it is clear in figure 22, the pressure drop grows up in the new proposed models because of the long pathway of flow. Especially in the M2 model, the

pathway is longer, and so the pressure drop is higher. On the other hand, the M1 model has almost the same pressure drop with the base model.

Thus it can be concluded that the M1 model is a proper model from performance and pressure drop viewpoint. Also the pressure drop for different cell voltages has been presented, and there is no pressure oscillation versus cell voltage, and it can be concluded that the pressure drop does not depend on the cell voltage.

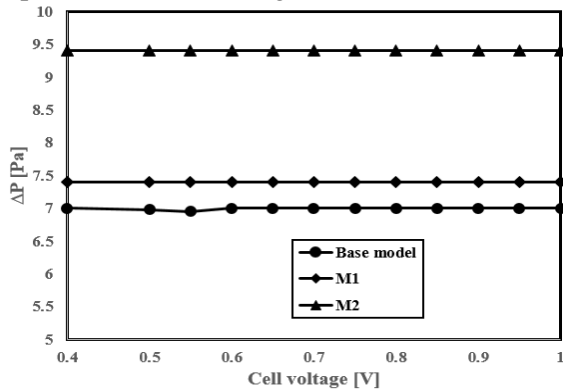


Figure 22. Pressure drop along the gas channel for different models at different cell voltages.

### 7.1. Bended model

In this section, the bended MEA effect on the cell performance and the mass transport phenomenon is studied. Table 3 shows the cell geometry properties. It should be said that the channel cross-section area has been kept constant for all models. Figure 23 illustrates the mentioned model with more details.

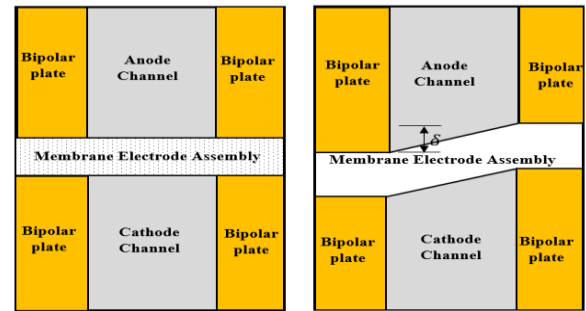


Figure 23. The base model (left) and bended model (right)

Figure 24 indicates the current density distribution along the cell between the cathode catalyst layer and the membrane (left) and also the average of mentioned parameter (right) at  $V = 0.4$  [V]. The results obtained declare that the model with  $\delta = 0.4$  has the maximum current density, so the oxygen consumption and consequently the water production will be higher. This fact can be found in figures 26 and 27. On the other hand, figure 25 shows the current density distribution for different  $\delta$  at  $Z = 18, 54$  mm. as it is clear, along the cell, the amount of current density has been decreased because of decrease in the electrochemical reaction rate. Also near the sharp edges of the bipolar plates, the current density is higher because there is the shortest path for electrons to reach the bipolar plates.

Table 3. Cell geometry properties.

Models	Reaction area	Channel cross-section area
$\delta = 0$	140 mm <sup>2</sup>	1 mm <sup>2</sup>
$\delta = 0.2$	145.39 mm <sup>2</sup>	1 mm <sup>2</sup>
$\delta = 0.4$	159.64 mm <sup>2</sup>	1 mm <sup>2</sup>
$\delta = 0.6$	179.4 mm <sup>2</sup>	1 mm <sup>2</sup>
$\delta = 0.8$	202.1 mm <sup>2</sup>	1 mm <sup>2</sup>

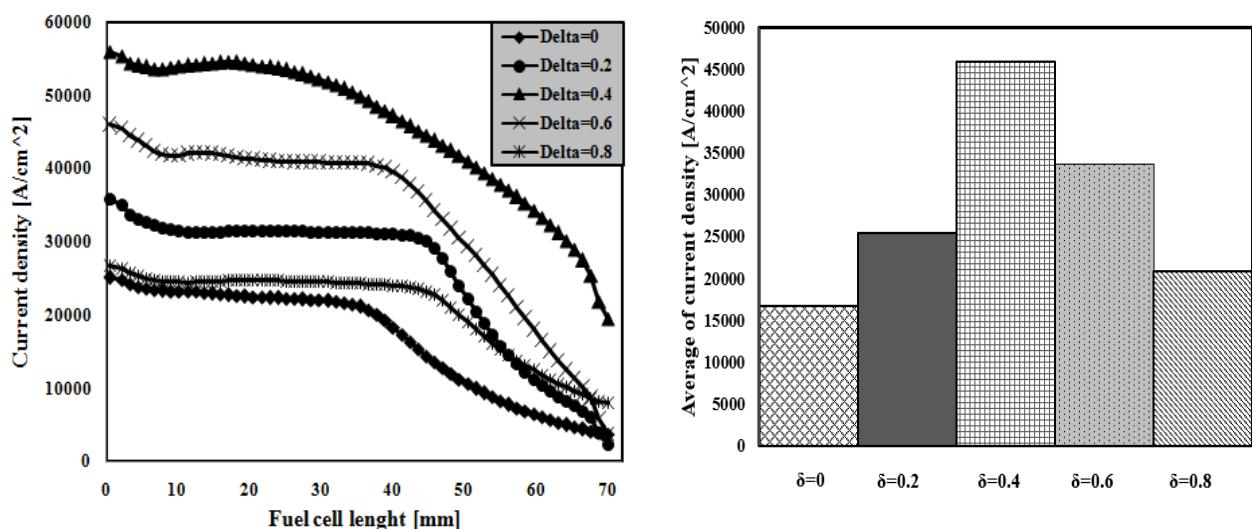


Figure 24. Current density distribution along the cell between cathode catalyst layer and membrane (left) and also the average of mentioned parameter (right).

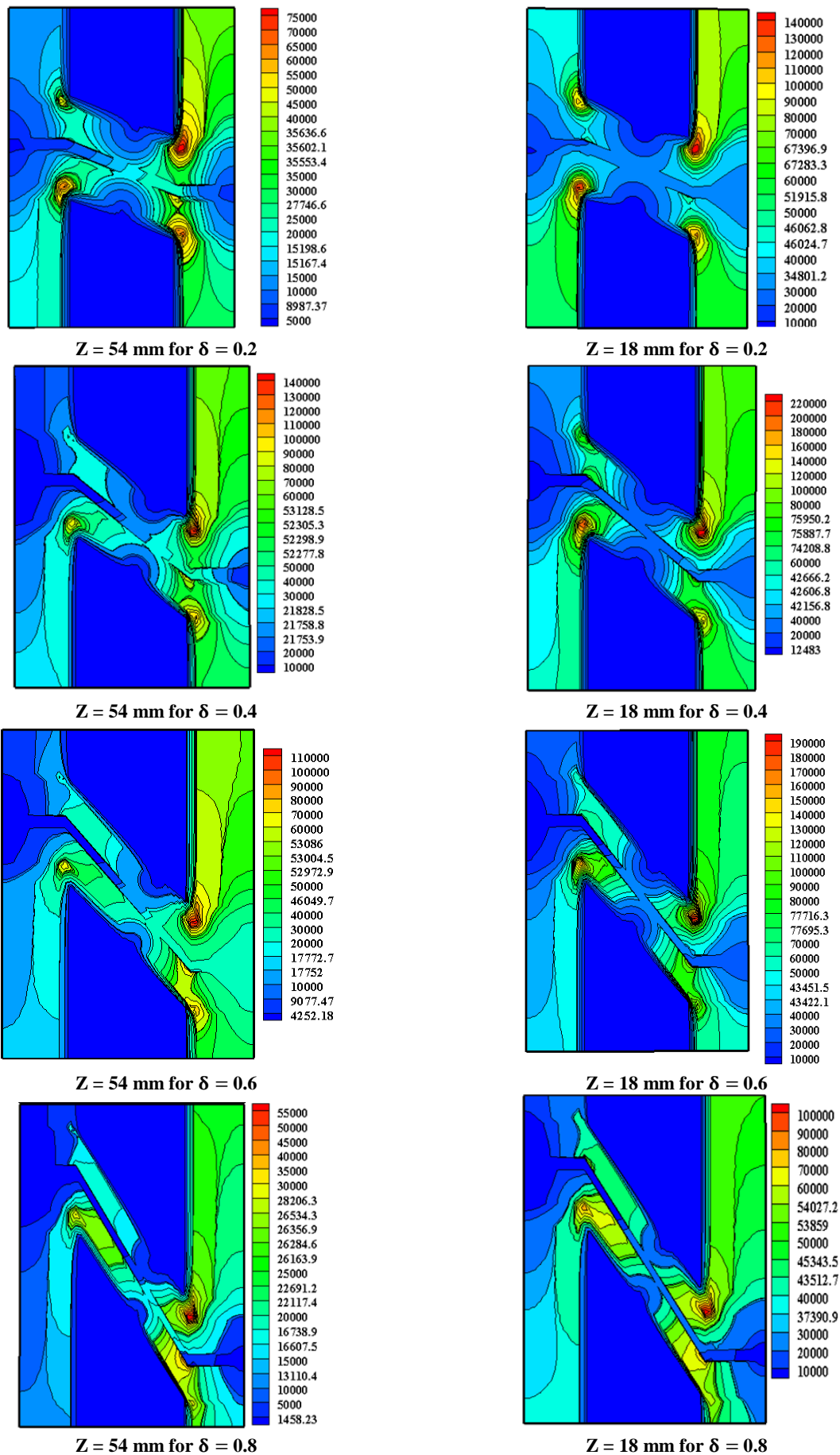


Figure 25. Current density distribution.

As mentioned earlier, the oxygen and water distribution shows a reasonable behavior. Thus for

the best model with  $\delta = 0.4$ , the water production and also, the oxygen consumption is higher.

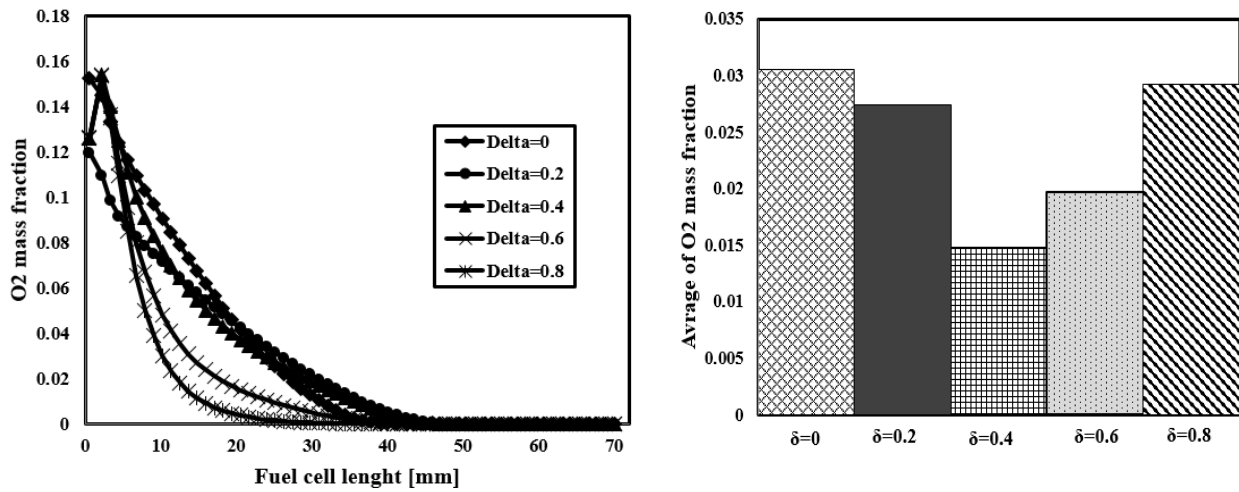


Figure 26. Oxygen distribution along the cell between cathode catalyst layer and membrane (left) and also the average of mentioned parameter (right).

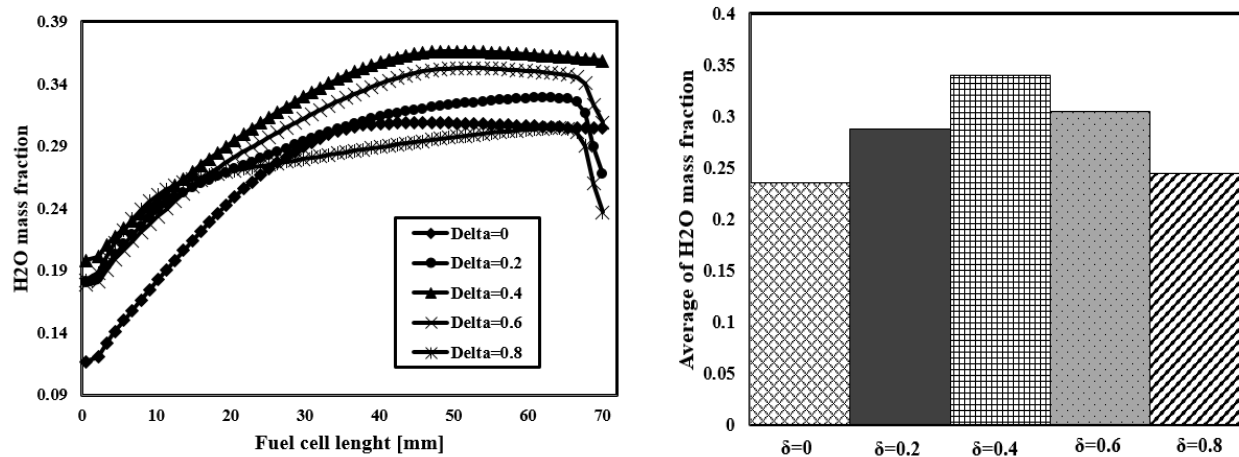


Figure 27. Water distribution along the cell between cathode catalyst layer and membrane (left) and also the average of mentioned parameter (right).

Figure 28 illustrates the temperature distribution. While there is a higher performance, because of a well electrochemical reaction rate, the generated

heat will be higher, so the temperature for the best model is higher than the other models.

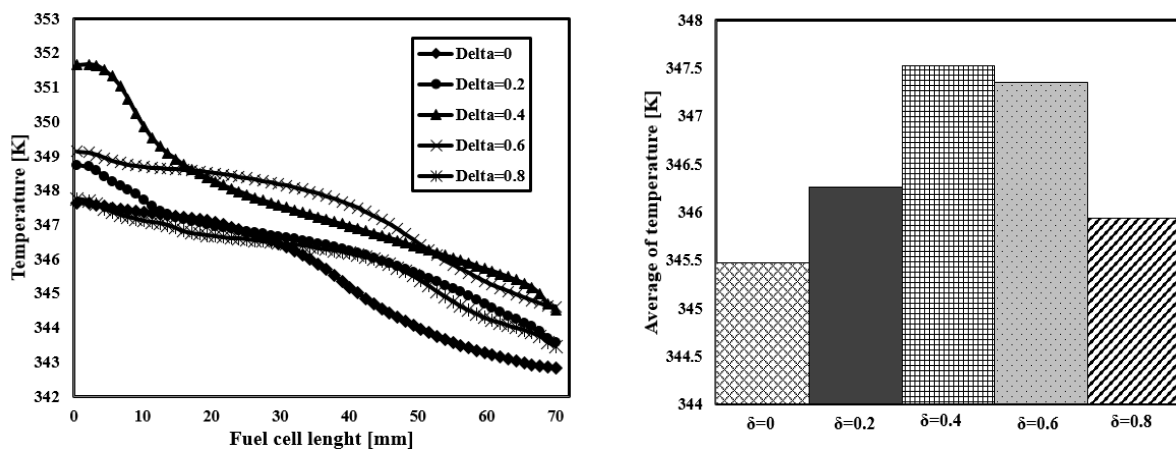


Figure 28. Temperature distribution along the cell between cathode catalyst layer and membrane (left) and also the average of mentioned parameter (right).

Figure 29 shows the temperature distribution for different  $\delta$  at  $Z = 18, 54$  mm at  $V = 0.4$  [V]. As it is clear, along the cell, the amount of temperature

has been decreased because of decrease in the electrochemical reaction rate and the cooling property of the produced water.

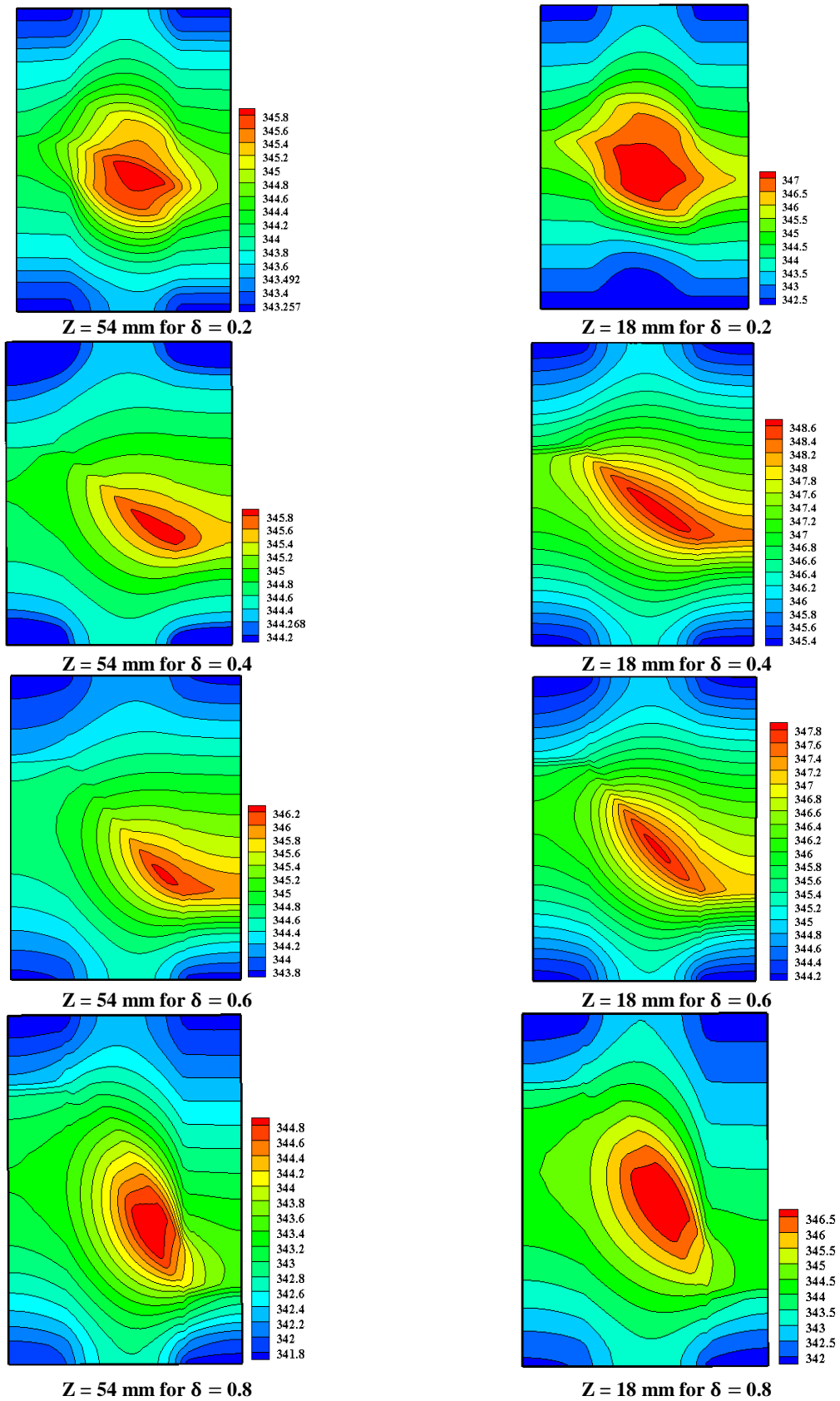


Figure 29. Current density distribution.

## 8. Conclusion

In the present work, at first, a base conventional model with straight gas channels was simulated, and in continuation, the two new proposed geometries for the gas channels were numerically studied with more details. The finite volume method for solving the governing equations was used, and verification of the obtained numerical results against the experimental data was illustrated. The results revealed that the novel models produced more current density than the base conventional model. For example, at  $V = 0.6$  [V], the model M1 increased the current density by 7.5% compared to the base model. Thus the proposed models consume more  $O_2$  and  $H_2$ , and also produce more water and heat. It means that the new structures that have been applied on fluid flow gas channels lead to a more output performance, which is an important advantage of the proposed models.

In the new models, the incoming gas path inside the cell gas channels is longer, so the mass diffusion toward the electrochemical reaction area enhances, which leads to a more current density extraction. Also changing the cross-section in mass moving direction such as expansion or contraction leads to a better mass distribution on GDL. Finally, the new proposed models of the fuel cell can be introduced as better cases for the users. Also in the new bended models, for  $\delta = 0.4$ , more performance has been extracted, while its electrochemical reaction area is  $19.64 \text{ mm}^2$  larger than the base model with  $\delta = 0$ . Meanwhile, in four new bended models, the gas channel cross-section area is constant and equal to  $1 \text{ mm}^2$ .

## Acknowledgment

We gratefully acknowledge the Urmia University Computer Center manager for allowance of using their computers.

## References

[1] Kreuer, K.D., editor, "Fuel cells", Springer, New York, (2013). <https://doi.org/10.1007/978-1-4614-5785-5>.

[2] Sajjad Rezazadeh, Iraj Mirzaee, Nader Pourmahmoud, Nima Ahmadi "Three Dimensional Computational Fluid Dynamics Analysis of a Proton Exchange Membrane Fuel Cell". Journal of Renewable Energy and Environment., Vol. 1, No. 1, (2014),30-42.

[3] N. Ahmadi, S. Rezazadeh, A. Dadvand, I. Mirzaee "Numerical Investigation of the Effect of Gas Diffusion Layer with Semicircular prominences on Polymer Exchange Membrane Fuel Cell Performance and Species Distribution". Journal of Renewable Energy and Environment., Vol. 2, No. 2, (2015),36-46.

[4] Nima Ahmadi, Abdolrahman Dadvand, Iraj Mirzaei, Sajad Rezazadeh. "Modeling of polymer electrolyte membrane fuel cell with circular and elliptical cross-section gas channels: A novel procedure". International Journal of Energy research., Vol. 42, No. 8, (2018), 2805-2822. <https://doi.org/10.1002/er.4069>.

[5] Zhuqian Zhang, Wei Liu, Yulei Wang, "Three dimensional two-phase and non-isothermal numerical simulation of multi-channels PEMFC", International journal of hydrogen energy, Vol. 44, (2018), 379-388. <https://doi.org/10.1016/j.ijhydene.2018.05.149>.

[6] Dutta, S., Shimpalee, S., Van Zee, JW. "Three-dimensional numerical simulation of straight channel PEM fuel cells", Journal of Applied Electrochemical, Vol. 30, (2000), 135-146. <https://doi.org/10.1023/a:1003964201327>.

[7] Chin T-san Wang., "A modified serpentine flow slab for in Proton Exchange Membrane Fuel Cells", Journal of Energy Procedia, Vol. 142, (2017), 667-673. <https://doi.org/10.1016/j.egypro.2017.12.110>.

[8] Tae-Hyun Yang, Gu-gon Park, Perumal Pugazhendhi, Won-Yong Lee, Chang Soo Kim, "Performance Improvement of Electrode for Polymer Electrolyte Membrane Fuel Cell", Korean journal of Chemical Engineering, Vol. 19, No. 3, (2002), 417-420. <https://doi.org/10.1007/bf02697149>.

[9] Akbar Mohammadi-Ahmar , Behzad Osanloo, Ali Solati , Jalal Ghasemi., "performance improvement of the circular tubular PEMFC by using different architectures and number of layers", Energy conversion and management, Vol. 128, (2016), 238-249. <https://dx.doi.org/10.1016/j.enconman.2016.09.074>.

[10] Carral, Ch., Mélé, P., "A Numerical Analysis of PEMFC Stack Assembly Through a 3D Finite Element Model", International Journal of Hydrogen Energy, Vol. 39, No. 9, (2014), 4516-4530. <https://doi.org/10.1016/j.ijhydene.2014.01.036>.

[11] Ahmadi N., Rostami S, "Enhancing the performance of polymer electrolyte membrane fuel cell by optimizing the operating parameter", Journal of Brazilian Society of Mechanical Science and Engineering, (2019). <https://doi.org/10.1007/s40430-019-1720-0>.

[12] Rezazadeh, S., Ahmadi, N., "Numerical investigation of Gas Channel Shape Effect on Proton Exchange Membrane Fuel Cell Performance", Journal of the Brazilian Society of Mechanical Sciences and Engineering, (2014). <https://doi.org/10.1007/s40430-014-0209-0>.

[13] Ticianelli, E. A., Derouin, C. R. Redondo, A., Srinivasan, S., "Methods to advance technology of proton exchange membrane fuel cell", Journal of Electrochemical Society, Vol. 135, No. 9, (1988) 2209-2214. <https://doi.org/10.1149/1.2096240>.

[14] Ahmadi, N., Pourmahmoud, N., Mirzaee I., and Rezazadeh, S. "Three-dimensional computational fluid

dynamic study of effect of different channel and shoulder geometries on cell performance." *Australian Journal of Basic and Applied Sciences*, Vol. 5, No. 12, (2011), 541-556.

[15] Ahmadi, N., Rezazadeh, S., Mirzaee, I., and Pourmahmoud., N. "Three-dimensional computational fluid dynamic analysis of the conventional PEM fuel cell and investigation of prominent gas diffusion layers effect." *Journal of mechanical science and technology*, Vol. 26, No. 8, (2012), 2247-2257. <https://doi.org/10.1007/s12206-012-0606-1>.

[16] Wang, Lin, Attila Husar, Tianhong Zhou, and Hongtan Liu. "A parametric study of PEM fuel cell

performances." *International Journal of Hydrogen Energy*, Vol. 28, No. 11, (2003), 1263-1272. [https://doi.org/10.1016/s0360-3199\(02\)00284-7](https://doi.org/10.1016/s0360-3199(02)00284-7).

[17] Ahmadi, N., Rezazadeh, S., Mirzaee, I., "Study the effect of various operating parameters of proton exchange membrane." *Periodica Polytechnica. Chemical Engineering*, Vol. 59, No. 3, (2015), 221-235. <https://doi.org/10.3311/ppch.7577>.

[18] Ahmadi N., Rezazadeh S., Dadvand A., Mirzaee I., "Modelling of gas transport in proton exchange membrane fuel cells", *ICE*, Vol. 170, No. 4, (2017), 163-179. <https://doi.org/10.1680/jener.15.00015>.